Influence of long-range-transported pollution on the annual and diurnal cycles of carbon monoxide and ozone at Cheeka Peak Observatory

Peter Weiss-Penzias and Daniel A. Jaffe
Interdisciplinary Arts and Sciences, University of Washington, Bothell, Washington, USA

Lyatt Jaeglé and Qing Liang
Department of Atmospheric Sciences, University of Washington, Seattle, Washington, USA

Received 2 January 2004; revised 9 April 2004; accepted 6 May 2004; published 23 July 2004.

[1] We assess the importance of distant pollution sources on the marine background by combining measurements of carbon monoxide (CO) and ozone (O_3) with model simulations from the GEOS-CHEM chemical transport model and two types of back trajectories. Measurements were made over a complete annual cycle from March 2001 to May 2002 at Cheeka Peak Observatory (CPO) in Washington State. Data from an earlier campaign (March–April 1997 and 1998) were also incorporated. The seasonal cycles of CO and O_3 show a spring maximum and a summer minimum, consistent with other remote sites in the marine boundary layer. European and Asian pollution emission sources of CO, parameterized by GEOS-CHEM, were grouped into one category called "LRT," representing "long-range transport." LRT values produced good correlations with measured CO (monthly averaged $r = 0.60$, 6-hour averages) and were found to comprise between 15 and 60% of total CO, with higher values in winter/spring and lower values in the summer/fall. CO and O_3 observations were classified on the basis of these LRT values, creating two general categories: "more polluted" (LRT > 75th percentile from monthly distribution) and "less polluted" (LRT < 25th percentile). The difference between these two categories is a measure of the net Asian enhancement above the background and reaches a maximum in the spring of 30-ppbv CO and in the spring-fall of 7-ppbv O_3. The Asian O_3 enhancement peaked at an average of 4 ppbv from April to October, which is the time of year of greatest urban air quality concerns in North America. Numerous long-range transport "events" (defined by at least 24 continuous hours of LRT > 75% percentile) were observed throughout the year. Ozone behavior was quite complicated during these events, producing no consistent enhancements. Classification of the measurements with LRT values from GEOS-CHEM is compared to back trajectories, both isentropic and kinematic. Isentropic trajectories agree reasonably well with GEOS-CHEM between February and May in capturing the CO enhancements in air masses influenced by recent emissions but were found to be less useful from June to January. HYSPLIT kinematic trajectories were slightly better at capturing the Asian pollution events than isentropic trajectories but still missed an event during the summer completely that was verified by GEOS-CHEM. Possible reasons for poor trajectory performance in the summer and fall are discussed. Long-range transport appears not to affect the magnitude of the diurnal variability of O_3 measurements at CPO, which reflect daytime production of 2–4 ppbv/d. Rather, ship traffic in the vicinity of CPO, which supplies NO_x through combustion, likely plays a dominant role. *INDEX TERMS:* 0345 Atmospheric Composition and Structure: Pollution—urban and regional (0305); 0365 Atmospheric Composition and Structure: Troposphere—composition and chemistry; 0368 Atmospheric Composition and Structure: Troposphere—constituent transport and chemistry; *KEYWORDS:* long-range transport, GEOS-CHEM, trajectories

Citation: Weiss-Penzias, P., D. A. Jaffe, L. Jaeglé, and Q. Liang (2004), Influence of long-range-transported pollution on the annual and diurnal cycles of carbon monoxide and ozone at Cheeka Peak Observatory, *J. Geophys. Res.*, *109*, D23S14, doi:10.1029/2004JD004505.

0148-0227/04/2004JD004505$09.00

1. Introduction

[2] Long-range transport of ozone (O_3) and its precursors is a central issue to understanding the dispersion of anthropogenic pollution and the global perturbation of tropospheric photochemistry. O_3 is a significant pollutant at the surface because it is linked to health effects and vegetation damage at concentrations not far above ambient in most urban areas. Of particular concern is the background contribution to the local O_3 burden. Typical values of O_3 in the remote Northern Hemisphere range between 20 and 50 ppbv, depending on season and altitude [*Oltmans and Levy*, 1994]. Recent model estimates have suggested that in the summer as much as 7 ppbv of the North American O_3 burden comes from Asian and European fuel combustion [*Fiore et al.*, 2002]. Likewise, North American anthropogenic emissions are estimated to contribute up to 10 ppbv to European O_3 during the summer [*Li et al.*, 2002; *Langmann et al.*, 2003], which may have caused 20% of the violations of the European Council ozone standard (55 ppbv, 8-hour average) in 1997 [*Li et al.*, 2002]. Estimates of the European influence on background O_3 in Asia suggest a 1–3 ppbv contribution of O_3 from transcontinental transport [*Pochanart et al.*, 2003]. These examples point to the challenges in the effective design of air pollution control strategies for regions that are currently having difficulty with attainment.

[3] Estimates of the future economic growth in the east Asian region point to a dramatic increase in fossil fuel combustion. By 2020, China is expected to have a twofold to fourfold increase in NO_x emissions (from 1990 levels) due to rapid development of the transportation sector [*Elliott et al.*, 1997; *Streets and Waldhoff*, 2000]. This will likely increase the amount of O_3 exported to North America [*Jacob et al.*, 1999; *Yienger et al.*, 2000]. Numerous episodes of pollution of Asian origin have already been measured in the North Pacific and on the west coast of North America [*Jaffe et al.*, 1998, 1999, 2001, 2003a; *Kotchenruther et al.*, 2001a; *Price et al.*, 2003; *Jaeglé et al.*, 2003]. However, to what extent these episodes control the background seasonality of O_3 and other pollutants like carbon monoxide (CO) in the boundary layer is still unclear. In addition to episodes, there is also evidence that springtime background O_3 concentrations have risen by 30% over western North America since the 1980s [*Jaffe et al.*, 2003b].

[4] Most previous measurements of O_3 and its precursors in the northeastern Pacific have only been made in the springtime (March–May) in part because of a higher probability of seeing long-range transport compared to other seasons [*Jaffe et al.*, 1999, 2001; *Newell and Evans*, 2000; *Kotchenruther et al.*, 2001a; *Staudt et al.*, 2001; *Price et al.*, 2003; *Jaeglé et al.*, 2003; *Huebert et al.*, 2003; *Fuelberg et al.*, 2003]. This stems from relatively long lifetimes of O_3 and related species during spring and an increase in frontal activity in east Asia, whereby pollutants are lifted from the boundary layer for transport in the free troposphere [*Bey et al.*, 2001a; *Liu et al.*, 2003; *Jaeglé et al.*, 2003]. In contrast, very little is known about transpacific transport processes in other seasons. Summer in particular is when many populated regions in the United States have difficulty meeting the national ozone standard (84 ppbv, 8-hour average). Even a small increase from long-range transport would make attainment more difficult [*Jacob et al.*, 1999].

[5] In this study, we use CO and O_3 measurements from Cheeka Peak Observatory (CPO) and results from the GEOS-CHEM global chemical transport model to quantify the effect of Asian and European anthropogenic emissions on a relatively cleaner background. We present a comparison of GEOS-CHEM versus two types of back trajectories in their abilities to segregate air masses into cleaner and more polluted categories and to capture significant long-range transport events. Diurnal cycles of O_3 are also observed during the spring and summer and their relationship to ship emissions in the region is discussed.

2. Methods

[6] Measurements of CO and O_3 were conducted at Cheeka Peak Observatory (CPO) on the northwestern tip of the continental United States (48.3°N, 124.6°W, 480 m above sea level, see map in Figure 1). The site is on a ridge top approximately 5-km inland of the Pacific Ocean in a very remote area with minimal sources of pollution in the immediate surroundings. CPO consistently lies in the marine boundary layer and during periods of westerly flow, there is little influence from recent North American emissions. Oceangoing ships, however, have a sporadic influence on the concentrations of NO_x and aerosols at the site, but do not appreciably affect CO [*Jaffe et al.*, 2001]. The climate is marine temperate with over 200 cm of rainfall a year, about 80% of which falls between November and April. During periods of easterly flow, the site receives polluted air from the populated Vancouver-Seattle-Portland corridor. These periods are easily detectable by increases in CO, particle scattering, radon, and other continental tracers [*Weiss-Penzias et al.*, 2003]. The site has been used for atmospheric chemistry and aerosol research for nearly 20 years [*Anderson et al.*, 1999]. The data used in this paper were collected from March 2001 to May 2002 (Photochemical Ozone Budget of the Eastern North Pacific Atmosphere (PHOBEA) II). In addition, we use data from March and April of 1997 and 1998 (PHOBEA I, previously reported by *Jaffe et al.* [1999, 2001]). The period of March–May 2002 corresponded with the Intercontinental Transport and Chemical Transformation 2002 (ITCT 2K2) campaign (D. D. Parrish et al., Intercontinental Transport and Chemical Transformation 2002 (ITCT 2K2) and Pacific Exploration of Asian Continental Emission (PEACE) Experiments: An overview of the 2002 winter and spring intensives, submitted to *Journal of Geophysical Research*, 2004).

[7] CO and O_3 were measured using the same methods as previous campaigns [*Jaffe et al.*, 2001]. Briefly, both species were measured from a common inlet situated atop a 10 m tower. The gases were sampled through 15 m of $\frac{1}{4}''$ OD Teflon tubing. The sample stream was teed with one side going to a nondispersive infrared CO instrument (API-300, Advanced Pollution Instruments, San Diego, California) and the other going to a standard UV absorbance O_3 analyzer (Dasibi 1008 RS). The CO instrument was modified to reduce water vapor interference and improve detection limits [*Jaffe et al.*, 1998]. The CO instrument was calibrated daily using a National Institute of Standards and Technology traceable standard and the O_3 instrument was calibrated quarterly using an ozone generator (Columbia Scientific),

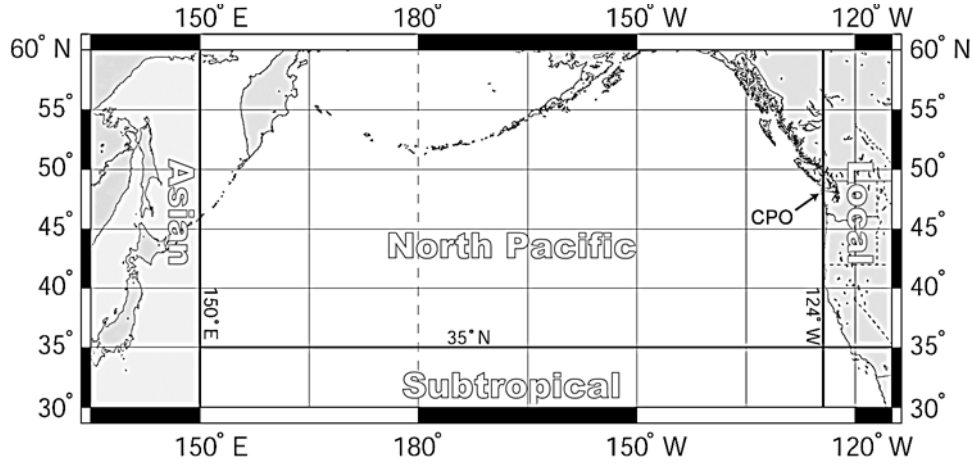

Figure 1. Location of CPO on the western coast of North America and the trajectory classifications based on air position criteria explained in text.

which was calibrated against a Washington Department of Ecology primary standard. In 2001, another Dasibi O_3 instrument from our lab was used as a transfer standard to check the accuracy of our O_3 calibrations. The precision of the CO and O_3 instruments was similar to that reported previously [*Jaffe et al.*, 2001] at 9% and 2%, respectively for an hourly average. The accuracy of these measurements over the 6-year period spanning the data set, due to calibration errors and standard drifts, is estimated to be better than 5%.

[8] Similar to our previous analyses [*Jaffe et al.*, 1999, 2001; *Kotchenruther et al.*, 2001a] isentropic 10-day back trajectories were calculated for CPO at 0 and 12 GMT for each day of the measurement periods [*Harris and Kahl*, 1994], using the Level III-B Basic Consolidated Data Set from the European Centre for Medium-Range Weather Forecasts (ECMWF). These meteorological fields have a 6-hour time resolution, and a horizontal resolution of 2.5° latitude × 2.5° longitude with 23 vertical layers. We also used 10-day back trajectories from the Hybrid Single-Particle Lagrangian Integrated Trajectory (HYSPLIT_4) model (hereafter referred to HYSPLIT kinematic trajectories) (HYSPLIT, NOAA Air Research Laboratory, Silver Spring, Maryland, available at http://www.arl.noaa.gov/ready/hysplit4.html, 1997) during selected long-range transport events as an accuracy check against isentropic trajectories. The HYSPLIT kinematic trajectory model was operated with the National Center for Environmental Prediction's (NCEP) FNL meteorological data set, which has a time resolution of 6 hours, and a horizontal resolution of 191 km with 13 vertical layers. These trajectories were also calculated at 0000 and 1200 GMT.

[9] While there are known problems with assumptions associated with the isentropic approach (such as near the surface and in the presence of precipitation) [*Stohl*, 1998, and references therein], there are numerous examples in the literature where it has been used successfully for chemical transport analyses [*Merrill*, 1994; *Moody et al.*, 1995; *Simmonds et al.*, 1997; *Harris et al.*, 2000; *Jaffe et al.*, 2001]. The HYSPLIT kinematic approach uses the three-dimensional wind components to generate its trajectories, which have been observed to give more realistic vertical and horizontal displacements than the isentropic approach [*Fuelberg et al.*, 1996].

[10] Trajectories arriving at CPO were classified in one of four ways (see map in Figure 1): those that crossed east of 124°W were called "local," those that crossed south of 60°N and west of 150°E were called "Asian," those that crossed south of 35°N were called "subtropical" (ST), and all other trajectories were called "North Pacific" (NP). The "Asian" region extends 10° farther north than that used by *Jaffe et al.* [2001] since it has been recognized that Asian outflow shifts northward during the summer and fall [*Liang et al.*, 2004].

[11] The GEOS-CHEM global chemical transport model was also used, which is a global three-dimensional model of tropospheric chemistry [*Bey et al.*, 2001b], driven by assimilated meteorological data for the specific years of this study, compiled at the Goddard Earth Observing System (GEOS) of the NASA Global Modeling and Assimilation Office (GMAO). The spatial resolution is 2° latitude × 2.5° longitude in the horizontal, with 30 vertical levels for the 2001/2002 runs and 26 vertical layers for the 1997/1998 runs. Surface meteorological fields have a 3-hour time resolution and upper level fields have a 6-hour time resolution. In this work, we have used 6-hour averages from a CO-only simulation using archived monthly OH fields from a full chemistry run [*Bey et al.*, 2001a; *Li et al.*, 2002]. Modeled CO is "tagged" by its sources and regions, which include Asian, European, and North American fossil fuel, biofuel, and biomass burning, as well as oxidation of methane, isoprene and other volatile organic compounds (VOCs) (B. N. Duncan et al., manuscript in preparation, 2004). This model has shown very good agreement with CO measurements from the "marine" and "continental" sectors at CPO using ground-based and vertical profile data from spring 2001 [*Jaeglé et al.*, 2003]. Further information about the GEOS-CHEM simulation used in this work is given by *Liang et al.* [2004].

3. Results and Discussion

3.1. Measurements

[12] In this paper, we focus on the marine air masses at CPO, which were identified using locally measured wind directions (between 160° and 315°), wind speeds (greater than 2 m/s), and isentropic back trajectories that showed the

Table 1. Monthly Means of CO and O_3 Measurements and GEOS-CHEM Model Results From "Marine-Only" Periods During the PHOBEA I and II Campaigns[a]

Month	Number of Hours "Marine-Only," Normalized by Month	Measured CO, ppbv	Measured O_3, ppbv	Total Modeled CO, ppbv	Measured CO Versus Total Modeled CO Corr. Coeff. *r*
Jan.	420	138	43.9	127	0.74
Feb.	282	149	44.2	134	0.70
March	380	159	44.8	147	0.60
April	395	154	45.8	142	0.79
May	516	132	44.6	120	0.59
June	534	103	36.6	102	0.50
July	630	81	28.4	94	0.16
Aug.	420	78	29.3	80	0.54
Sept.	288	87	34.2	97	0.42
Oct.	450	ND	41.4	109	ND
Nov.	408	112	42.4	117	0.60
Dec.	372	129	43.5	124	0.24
Annual average, normalized	425 (59%)	120	39.9	116	0.53

[a]Six-hour averages were used for both the measurements and the model. ND refers to no CO measurements. Corr. coeff., correlation coefficient.

air had not crossed east of 124°W [*Jaffe et al.*, 2001]. All model results were segregated in an identical fashion. In this paper, the terms "marine," "marine-only," and "background" are used interchangeably. Table 1 shows the number of hours in each month that were classified as "marine." These vary from a low of 282 hours (42%) in February to a high of 630 hours (85%) in July, with an annual average of 425 hours or 59% of the time. March, April, and May represent more than 1 year's worth of data but have been normalized to a monthly average. In general, winter and spring have less "marine" periods than the summer because of more frequent springtime surface high-pressure systems that produce low-level easterly flow. In addition, there are fewer storms during the summer months resulting in a more consistent onshore flow.

[13] The three sources of data used here have different timescales (measurements, continuous hourly averages; GEOS-CHEM, 6-hour averages; and trajectories, every 12 hours). In comparing measurements with GEOS-CHEM, 3 hours of measurements before and after the time of the GEOS-CHEM data point were averaged. For comparison with trajectories, 6 hours of measurements before and after the time of the trajectory were averaged.

[14] Table 1 and Figure 2a show the monthly means of our CO and O_3 measurements during the PHOBEA I–II campaigns. CO measurements from October 2001 have been omitted since there was a three-week data gap due to instrument maintenance. The annual cycle of CO at CPO is similar to that of other Northern Hemisphere remote sites and consistent with the observed latitudinal gradient over the Pacific [*Novelli et al.*, 1992, 1998]. The spring maximum (March: 159 ppbv) and summer minimum (August: 78 ppbv) are primarily driven by the seasonal cycle in OH concentrations and the seasonality of transport processes [*Holloway et al.*, 2000]. Reaction with OH accounts for up to 95% of the global sink, which gives a CO lifetime of about one month in the summer and up to a year during the winter in the midlatitudes [*Novelli et al.*, 1998]. The North Pacific atmosphere is the most affected by direct Asian outflow of pollutants during the spring and the least affected during the summer [*Jacob et al.*, 2003]. This combined effect of chemistry and transport causes about a factor of 2 drop in CO concentration from spring to summer.

[15] The annual cycle of O_3 in Figure 2a also shows a spring maximum (April: 45.8 ppbv) and a summer minimum (July: 28.4 ppbv), and this general feature has been observed at other remote locations in the marine boundary layer (e.g., Mace Head, Ireland, and Bermuda) [*Oltmans and Levy*, 1994]. Long-range transport from pollution sources and the seasonality in OH also play important roles in the seasonality of surface O_3, producing a similarity to the CO cycle [*Parrish et al.*, 1998]. The O_3 budget is also influenced by downward transport from the stratosphere [*Moody et al.*, 1995], dry deposition to the sea surface [*Lelieveld and Dentener*, 2000], loss in clouds via aqueous chemistry [*Barth et al.*, 2002] and destruction by halogen radicals associated with sea salt aerosols [*Dickerson et al.*, 1999]. O_3 at CPO differs slightly from other marine boundary layer (MBL) sites in that the spring maximum is much less pronounced, with O_3 levels changing by <5 ppbv in the eight months between October and May, compared to about 10 ppbv for Mace Head and Bermuda over the same time period [*Oltmans and Levy*, 1994]. Part of the reason for the smaller spring increase at CPO could be the great distance between CPO and pollution sources to the west, which would allow for more thorough dilution of pollution plumes. Additionally, frequent wintertime storms at CPO could enhance O_3 levels because of deep mixing with the upper troposphere during the passage of cold fronts [*Kunz and Speth*, 1997].

3.2. Comparison of CO Measurements With GEOS-CHEM

[16] Shown in Figure 2a is a comparison between monthly means of measured and modeled CO. The model captures the general features of the annual cycle of CO quite well, peaking in March and reaching a minimum in August. The model shows a negative offset of about 8% from December to May, and a 10–15% positive offset from July to September, although the means generally fall within one standard deviation of one another. On an annual basis, the correlation between the model and measurements is quite strong ($r = 0.92$, using 6-hour averages), primarily because GEOS-CHEM captures the seasonal cycle of CO, which

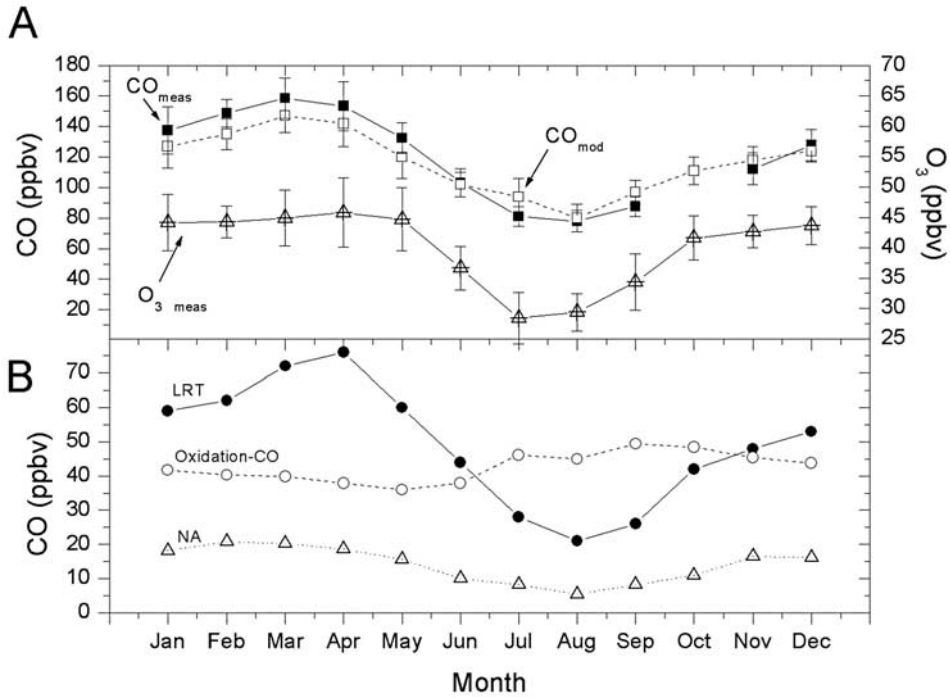

Figure 2. (a) Measured CO (CO_{meas}) and O_3 ($O_{3\ meas}$) and modeled CO (CO_{mod}) monthly means and standard deviations at CPO during PHOBEA I–II. Both model and measurements have been screened for "marine-only" periods. (b) Model-generated medians of CO from three sources. "LRT," Asian biomass burning + Asian and European fossil fuel and biofuel combustion; "oxidation-CO," oxidation of hydrocarbons; and "NA," fossil fuel combustion from North America.

drives the correlation. The average of each monthly correlation, shown in Table 1, is 0.53, with winter/spring providing the strongest correlations (r = 0.50 to 0.79) compared to summer/fall (r = 0.16–0.60). An overestimation of isoprene emissions in the model has been used to explain the poorer model performance in summer/fall at CPO [*Liang et al.*, 2004; *Abbot et al.*, 2003].

[17] Figure 2b shows the breakdown of CO sources (medians) in GEOS-CHEM: "LRT" (combination of Asian biomass burning, and Asian + European fossil fuel and biofuel combustion), "oxidation-CO" (oxidation of methane and biogenic VOCs), and "NA" (fossil fuel combustion from North America). LRT is the dominant source of CO at CPO between January and May, with a maximum of 76 ppbv (49%) in April. This arises from the relatively longer lifetime of CO in the winter/spring in conjunction with the dominance of westerly flow and entrainment of Asian emissions throughout the midlatitudes [*Jacob et al.*, 2003]. Asian biomass burning (included as part of LRT) is a minor contributor to total CO, comprising less than 6 ppbv (7%) at its maximum during the spring. Biomass-burning CO emissions in the model include interannual variability for the 1997 and 1998 simulations and are based on seasonally varying climatological values developed by *Duncan et al.* [2003] for the 2001 and 2002 simulations. Thus the model does not account for periodic strong enhancements of Siberian biomass emissions, as seen recently in the free troposphere by *Bertschi et al.* [2004] during the spring of 2002 and at the surface during the summer of 2003 (D. A. Jaffe, unpublished data, 2004). "Oxidation-CO" dominates from July to October, reaching a peak of 50 ppbv (56%) in August. The seasonality of oxidation-CO is largely a function of OH, in addition to the increase in biogenic emissions of isoprene during the Northern Hemisphere growing season. NA represents CO that has undergone circumpolar transport and arrives at CPO from the west, since the data set has been screened to eliminate direct easterly transport to the site. NA reaches its peak in the winter/spring at 22 ppbv (15%) of the total in February, primarily because of the longer lifetime of CO in the winter.

3.3. Using LRT From GEOS-CHEM to Segregate CO and Ozone Measurements

[18] In this section, we investigate the degree to which measured CO at CPO can be explained by the LRT parameter. Table 2 shows the monthly correlation coefficients r between these two quantities, giving a monthly average of r = 0.60. As with total modeled CO, the strongest correlations occur between January and August. This points to the importance of LRT in controlling the variability of CO during this part of the year. Later in the fall, CO-LRT correlations weaken largely because the model then attributes lower importance to LRT.

[19] For each month, we have used the distribution of LRT values as a segregation tool for CO and O_3 observations. The 75th and 25th percentile values of LRT have been somewhat arbitrarily selected for identifying time periods of relatively "polluted" or "clean" air from the marine sector, respectively. This is analogous to data segregation using back trajectories [e.g., *Simmonds et al.*, 1997; *Derwent et al.*, 1998; *Jaffe et al.*, 1999, 2001] to identify distinct source regions, based on the likely path of an air mass before

Table 2. Long-Range Transport (LRT) Component From GEOS-CHEM and Its Correlation With Measured CO[a]

Month	Measured CO Versus LRT Correlation r	LRT Median, ppbv	LRT 75th Percentile, ppbv	LRT 25th Percentile, ppbv	Difference Between 75th and 25th Percentiles, ppbv
Jan.	0.71	59	61	55	6
Feb.	0.69	62	66	55	11
March	0.55	72	81	69	12
April	0.74	76	80	67	13
May	0.66	60	66	49	17
June	0.70	44	47	34	13
July	0.60	28	30	25	5
Aug.	0.60	21	25	18	7
Sept.	0.47	26	30	25	5
Oct.	ND	42	45	39	6
Nov.	0.47	48	51	43	8
Dec.	0.37	53	56	50	6
Annual average, normalized	0.60	49	53	44	9

[a]All data are calculated using 6-hour averages. ND refers to no CO measurements.

measurement. However, segregating the data on the basis of LRT > 75% and LRT < 25% criteria incorporates mixing, chemical processing, and emission strengths in addition to the geographical origin of an air mass. As will be shown below, this produces a better agreement with the measurements compared to using either the isentropic or HYSPLIT kinematic trajectories.

[20] The strength of the segregation between polluted and clean categories, how distinct these categories are from one another, is indicated by the variability of LRT in a given month. This variability can be seen in the monthly probability distribution of LRT values, shown in Figure 3. The medians of these distributions correspond to the LRT values presented in Figure 2b. The median, 75th percentile, and 25th percentile LRT values are shown in Table 2. The difference between the 75th percentile and 25th percentile values reaches a maximum in May (17 ppbv) and a minimum in July and September (5 ppbv). May variability is largely caused by the seasonal cycle of CO, which results in a dramatic drop in LRT values from the first to the last parts of May. On a seasonal basis, LRT > 75% minus LRT < 25% values display the highest variability from February to June (11–17 ppbv) compared to July–January (5–8 ppbv). This higher variability in the spring is consistent with the seasonality of meteorological patterns over the Pacific, which favor more rapid transport followed by relatively quiescent periods [*Yienger et al.*, 2000; *Liu et al.*, 2003; *Jacob et al.*, 2003]. In addition to these ''episodes,'' however, we also point out that so-called ''clean'' conditions at CPO, particularly in the spring, do not exist. Figure 3 shows that LRT during March and April is rarely less than 50 ppbv (about one third of the total CO).

[21] During months with very low LRT variability (July–January), our ''cleaner'' and ''more polluted'' categories are only weakly separated, and approach the uncertainty of the CO measurements (9% uncertainty in an hourly average, or 4% in a 6-hour average). Thus, on the basis of LRT values alone, we can only tentatively assign the measurements to different categories in the months where LRT is low and/or less variable. However, in spite of these limitations, we are able to identify some specific events consistent with the observations, which are largely missed using trajectory classifications alone.

[22] The results of segregating CO and O_3 measurements using LRT > 75% and LRT < 25% are shown in Figure 4,

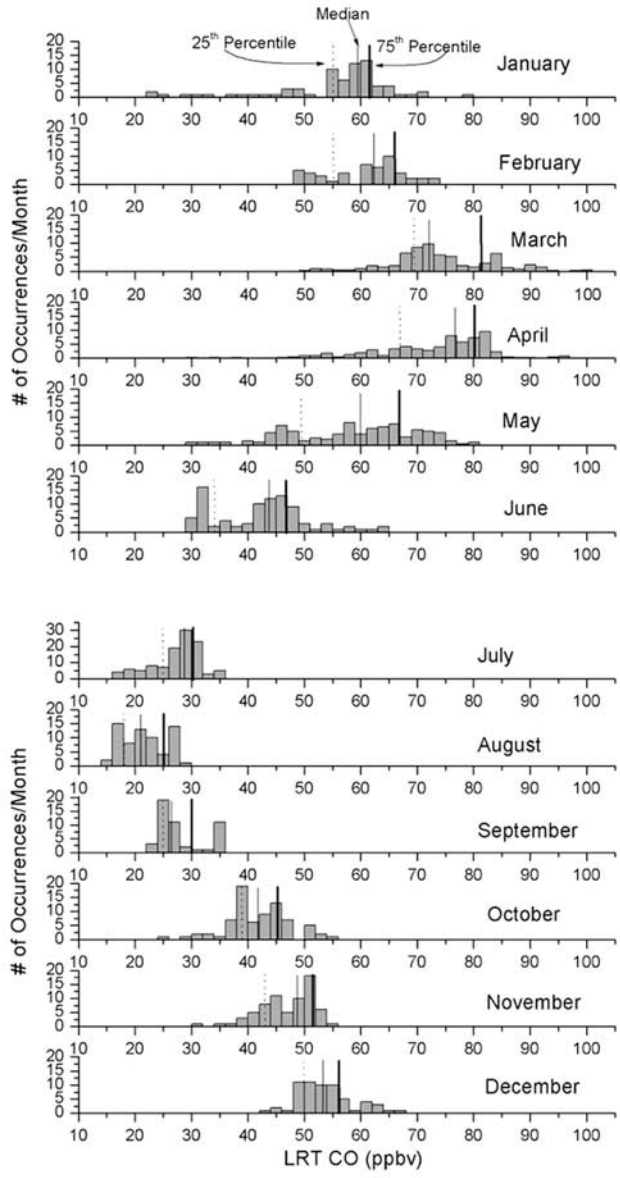

Figure 3. Histograms of LRT CO values for each month, using 6-hour-averaged marine-only LRT data. The median and 75th and 25th percentiles are shown, which correspond to the data in Table 2. Note the different y axis scale for July.

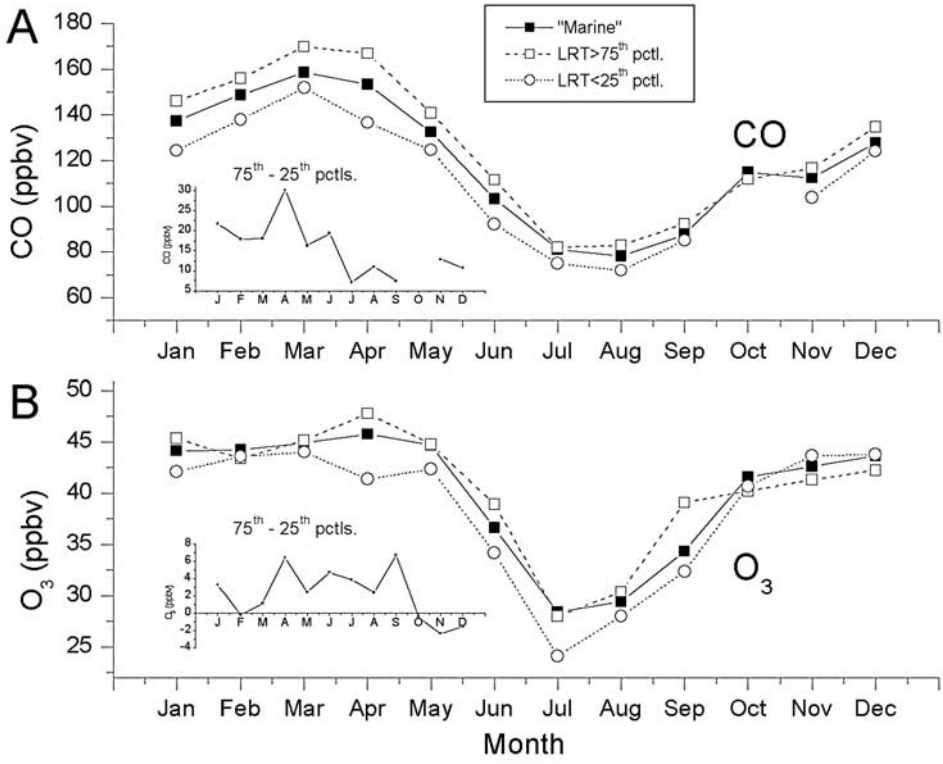

Figure 4. Monthly averages of (a) measured CO and (b) measured O_3 concentrations segregated by the amount of "LRT" predicted by GEOS-CHEM. The inset graphs show the difference in CO and O_3 concentrations between the high (>75th percentile) and low (<25th percentile) LRT categories.

along with all marine data. Figure 4a shows that LRT > 75% CO measurements (CO_{LRT75}) are higher in every month than LRT < 25% measurements (CO_{LRT25}), providing a reasonable measure of validation to our method. The difference between these two classifications can be seen in the inset of Figure 4b, reaching a peak of 30 ppbv in April. This is a measure of the Asian enhancement above the background. The January–June enhancement (23 ppbv) is significantly higher than that for July–December (10 ppbv), consistent with the model results (Table 2). This indicates that the first part of the year, and particularly during April, variability in long-range transport plays a larger role in controlling CO concentrations at CPO than later in the year.

[23] Figure 4b shows the data segregation results for O_3. Here the difference between $O3_{LRT75}$ and $O3_{LRT25}$ reveals a different seasonality compared to CO. The peak for O_3 occurs in April and September at nearly 7 ppbv, with the six-month period of April–October showing the greatest average difference (4.4 ppbv) compared to November–March (0.0 ppbv). This shows that while long-range transport of CO is strongest in winter/spring, O_3 from distant sources has its maximum influence much later in the year, coinciding with the summer smog season in urban areas of North America, as suggested by *Jacob et al.* [1999]. October–December and February show no apparent Asian contribution of O_3, even though the east Asian region is thought to be a net exporter of O_3 to the Pacific in all seasons [*Mauzerall et al.*, 2000]. This could be explained by urban titration of O_3 by NO_x in Asia, similar to the observations of *Parrish et al.* [1998] downwind of the eastern United States. However, O_3 loss in transit due to very low NO_x levels may also be important, combined with negligible O_3 production due to low in situ temperatures and light levels.

3.4. Using GEOS-CHEM to Identify Long-Range Transport Events

[24] There have been numerous observations of events at CPO and over the eastern Pacific [*Jaffe et al.*, 1999, 2001; *Kotchenruther et al.*, 2001a; *Fuelberg et al.*, 2003; *Huebert et al.*, 2003; *Price et al.*, 2003; *Jaeglé et al.*, 2003]. Here we use GEOS-CHEM results and our CO observations to identify events during all seasons at CPO, not just in spring, as has previously been the case. An event was determined if the following criteria were met: (1) model-generated LRT values reached >75th percentile for at least 24 hours continuously, (2) total modeled CO and measured CO were enhanced by a statistically significant ($P > 0.95$) amount above their respective monthly means, and (3) measured versus modeled CO correlations r were > 0.10. The duration of an event was identified in two ways: the total number of hours when LRT > 75%, and the time between LRT minima on both sides of the LRT maximum. This latter criterion was used for calculating ΔCO and ΔO_3 values, along with correlation coefficients. Table 3 shows a list of all events identified from our data set using these criteria. ΔCO refers to the difference between the event maximum (6-hour average) and the monthly mean. ΔO_3 is the difference between the measured O_3 value at the time of the measured

Table 3. Events of Long-Range-Transported Pollution Identified During the PHOBEA I and II Campaigns at CPO, Arranged Chronologically, and Compared to the GEOS-CHEM Model Results[a]

Event Date (Midpoint), GMT	Number of Hours LRT > 75	ΔCO, ppbv			ΔO_3, ppbv	Correlation *r*	
		Measured	Total Modeled[b]	LRT Modeled[c]		Modeled Versus Measured CO	Measured O_3 Versus CO
9 March 1997	78	24	20	19	−3.2	0.33	−0.30
29 March 1997	60	19	21	20	1.2	0.77	0.42
11 March 2001	30	28	21	26	4.5	0.97	0.59
7 April 2001	54	16	13	9	−0.8	0.64	−0.48
29 April 2001	30	4	8	11	9.3	0.75	0.49
2 May 2001	60	19	25	20	1.2	0.31	−0.10
12 July 2001	*48*	*5*	*27*	*3*	*−2.4*	*0.59*	*−0.23*
16 July 2001	*54*	*7*	*4*	*6*	*−1.7*	*0.61*	*−0.09*
28 Sept. 2001	**78**	**18**	**20**	**9**	**2.2**	**0.75**	**−0.19**
21 Nov. 2001	**30**	**10**	**7**	**6**	**1.6**	**0.21**	**−0.05**
5 Dec. 2001	***54***	***16***	***13***	***14***	***−2.9***	***0.30***	***0.55***
9 Jan. 2002	***24***	***3***	***12***	***6***	***6.2***	***0.92***	***0.88***
20 Jan. 2002	***66***	***28***	***23***	***20***	***2.6***	***0.81***	***−0.13***
27 March 2002	24	24	22	28	2.1	0.79	−0.04
4 May 2002	48	16	14	16	1.7	0.18	0.05
15 May 2002	42	8	15	12	−6.4	0.24	−0.46
All events, weighted by number of hours	774	16	17	14	0.4	0.91	0.78

[a]See text for definition of events. ΔCO refers to the maximum difference between a 6-hour average and the monthly mean. ΔO_3 refers to the difference between the 6-hour average and the monthly mean, at the same time as the measured CO maximum. The seasons are shown with roman type for spring, italic type for summer, bold type for fall, and bold-italic type for winter.
[b]Total modeled CO.
[c]LRT component of total modeled CO.

CO event maximum, and the monthly O_3 mean. There is good agreement between total modeled and measured CO during the events as shown by the correlation coefficients in Table 3. Table 4 shows a list of events that met the first criteria but not both criteria 2 and 3, and will be discussed below. The date of each event refers to the approximate midpoint (GMT).

[25] Typographical emphasis has been added to Table 3 to indicate the season of each event, showing that there are three to four events in spring, two events in summer, two events in fall, and three events in winter. There is no clear seasonal trend in the duration of events, with times ranging from 24 to 78 hours of LRT > 75%. However, there is a seasonal trend in the magnitude or strength of these events, as shown by the lack of an event with $\Delta CO_{meas.} > 20$ ppbv during the summer and fall. This is consistent with our view of winter and spring as being more influenced by long-range transport, and summer/fall being a more quiescent period. A number of events seen here have been reported elsewhere: 29 March 1997 [*Jaffe et al.*, 1999], 11 March 2001 [*Jaeglé et al.*, 2003], 20 January 2001, 27 March 2002, and 15 May 2002 [*Liang et al.*, 2004; *Price et al.*, 2004].

[26] Table 3 shows that O_3 is not significantly enhanced, taking the time-weighted average of all events. It also does not appear to follow any particular seasonal trend, which is somewhat confusing. On the basis of our GEOS-CHEM segregation results in Figure 4a, we would expect late spring/summer events to bring enhanced O_3. However, the two events in July both brought a drop in O_3 concentrations, and a negative O_3-CO correlation. The event on 15 May 2002 brought the largest O_3 decrease of any event (−6.4 ppbv). Large O_3 enhancements (>4 ppbv) also occur in some events, restricted to spring and winter. The high degree of O_3-CO correlation for all events taken together is a function of the similarity in the O_3 and CO seasonal cycles, rather than many individual events having strongly positive correlations. As has been noted previously, air masses with clear anthropogenic signatures do not always contain O_3 enhancements [*Jaffe et al.*, 2003a]. O_3 behavior can be complicated by the presence of mineral dust [*He and Carmichael*, 1999], destruction during transit over the ocean, or the possible mixing with stratospheric O_3 [*Carmichael et al.*, 1998]. In fact, the 29 April 2001 and 9 January 2002 events showed relatively large O_3 increases and were associated with dry air and relatively

Table 4. Events Predicted by GEOS-CHEM but That Do Not Agree Well With the Observations[a]

Event Date (Midpoint), GMT	Number of Hours LRT > 75%	ΔCO, ppbv			Modeled Versus Measured CO Correlation	Reason for Disagreement
		Measured	Total Modeled	LRT Modeled		
20 March 1997	30	−5	12	13	0.94	M
2 April 2001	36	23	16	6	−0.13	C
11 June 2001	*72*	*9*	*18*	*21*	*0.02*	*C*
4 Aug. 2001	*30*	*2*	*16*	*7*	*−0.07*	*M, C*
24 Aug. 2001	*54*	*15*	*21*	*7*	*−0.77*	*C*
23 April 2002	48	19	21	20	−0.75	C

[a]Under "Reason for Disagreement," M refers to a lack of significant increase in measured CO, and C refers to poor correlation between model and measurement. The definition of ΔCO and the roman/italic type indicating season are identical to that in Table 3. Six-hour averages were used to calculate *r*.

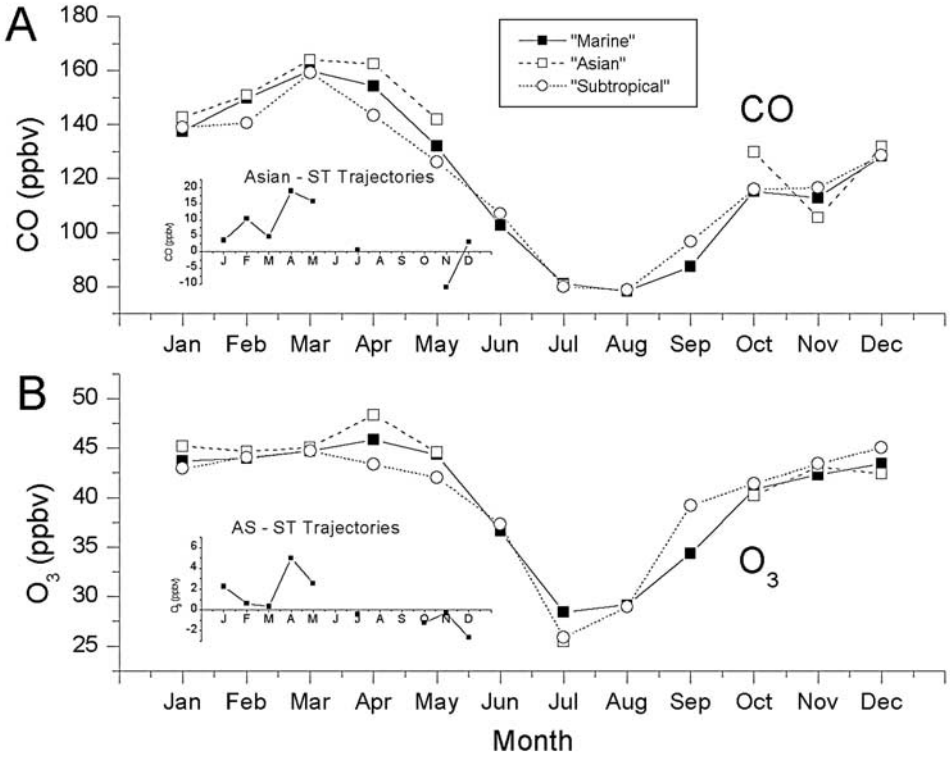

Figure 5. Monthly averages of (a) measured CO and (b) measured O_3 concentrations segregated with isentropic back trajectories, defined by the regions shown in Figure 1. The inset graphs show the difference in CO and O_3 concentrations between the "Asian" and "subtropical" categories. Data gaps in the inset graphs represent months where no "Asian" trajectories were classified.

small CO increases, which suggests a possible stratospheric influence.

[27] Three events in both spring and summer were predicted by GEOS-CHEM, but did not produce a good correlation with the measurements and/or did not result in a significant increase in measured CO. These are listed in Table 4. In most cases, GEOS-CHEM accurately predicted the presence of enhanced pollution, but missed the exact timing of the event, leading to an insignificant or even negative correlation. Only in two cases, did GEOS-CHEM appear to predict an event that was not observed at all (20 March 1997 and 4 August 2001). The 23 April 2002 case has been reported by *Liang et al.* [2004] and is an example of a time when measured CO peaked and dropped rapidly about 24 hours before the maximum in LRT and total modeled CO. This resulted in a correlation of $r = -0.75$, even though the magnitude of the observed CO increase agrees very well with the model.

3.5. Comparison of GEOS-CHEM With Back Trajectories

[28] In this section we compare isentropic and HYSPLIT kinematic trajectories with GEOS-CHEM; both in their ability to accurately segregate CO/O_3 measurements into cleaner and more polluted categories and to capture individual events. Isentropic trajectories were calculated every 12 hours throughout the entire time period of the measurements and HYSPLIT kinematic trajectories were calculated during selected events for the purposes of checking the accuracy of the simpler isentropic model. In comparing trajectories to GEOS-CHEM, LRT > 75% from the previous sections is analogous to "Asian" trajectories and LRT < 25% is analogous to "subtropical" trajectories, as defined in section 2. Part of the motivation for such a comparison is that some of our current and past work has relied upon using both isentropic and HYSPLIT kinematic back trajectories [*Price et al.*, 2004; *Bertschi et al.*, 2004; *Kotchenruther et al.*, 2001a; *Jaffe et al.*, 1999, 2001] and we wish to assess their performance relative to a global chemical tracer model. However, it should be noted that air mass pathways from GEOS-CHEM might be quite different from those obtained from trajectories, merely because of the different types of meteorological data being used as inputs to each model. Each data set has a different spatial and temporal resolution, which may lead to different conclusions about the degree of Asian influence [*Pickering et al.*, 1996; *Fuelberg et al.*, 1996]. Thus, even though we feel that the following comparison between GEOS-CHEM and trajectories shows a general limitation of trajectories for this type of analysis, we must keep in mind that our results could be sensitive to model input parameters.

[29] In Figure 5 we present the results from an isentropic trajectory segregation of the monthly averaged CO and O_3 measurements, where the format is identical to Figure 4. At first glance, isentropic trajectory segregation produces some of the same results as those obtained with GEOS-CHEM. The inset of Figure 5a shows that Asian CO is larger than ST CO in most months, especially spring, where the difference

Table 5. Number of Hours During Long-Range Transport Events That Were Classified as "Asian" by Isentropic and HYSPLIT Kinematic Trajectories, in Comparison to the Number of Hours LRT > 75%[a]

Event Date (Midpoint), GMT	Number of Hours LRT > 75%	Number of Hours Isentropic	Number of Hours HYSPLIT Kinematic
9 March 1997	78	72	72
29 March 1997	60	36	60
11 March 2001	30	24	24
27 March 2002	24	24	24
7 April 2001	54	12	12
29 April 2001	30	24	24
2 May 2001	60	24	12
4 May 2002	48	24	24
15 May 2002	42	0	12
March–April total	276	192 (70%)	216 (78%)
Spring total	426	240 (56%)	264 (62%)
12 July 2001	48	0	0
16 July 2001	54	12	24
Summer total	102	12 (12%)	24 (24%)
28 Sept. 2001	78	0	24
21 Nov. 2001	30	0	12
5 Dec. 2001	54	48	48
9 Jan. 2002	24	0	24
20 Jan. 2002	66	36	12
Fall/winter total	252	84 (33%)	120 (48%)
All events	774	336	408

[a]The totals for each season are given in hours and in the percentage of LRT > 75% hours.

reaches ~20 ppbv, which is comparable in timing and magnitude to the difference between CO_{LRT75} and CO_{LRT25} in Figure 4a. The Asian O_3/ST O_3 difference (Figure 5b) shows a spring maximum as well, which is in agreement with $O3_{LRT75}$ and $O3_{LRT25}$. The magnitude of the maximum Asian influence for O_3 is also comparable to that in Figure 4b (~5 ppbv). Springtime Asian pollution events are also fairly well captured by isentropic trajectories. We found that 56% of the total LRT > 75% hours during spring events corresponded to an Asian classification (Table 5). During March and April, isentropic trajectories captured 70% of the events. These demonstrated similarities to GEOS-CHEM in the spring give a measure of confidence to past studies at CPO that relied solely upon isentropic trajectories [*Jaffe et al.*, 1999, 2001; *Kotchenruther et al.*, 2001a].

[30] However, in contrast with GEOS-CHEM, isentropic trajectories do not provide much meaningful information from June to January. In particular, in Table 6 we see that from June to September, only one "Asian" isentropic trajectory was identified. To ascertain whether this lack of isentropic trajectories was due to a limitation associated with the isentropic model, we also calculated HYSPLIT kinematic trajectories for the Asian events as shown in Table 3. This comparison between HYSPLIT kinematic, isentropic, and GEOS-CHEM during these events is shown in Table 5. Here we see that both HYSPLIT kinematic and isentropic trajectories classify many fewer hours as "Asian" than GEOS-CHEM in summer (12–24%) and fall-winter (33–48%). While HYSPLIT kinematic generally captures more of each Asian pollution event and misses fewer events completely, it does not appear to be dramatically better than isentropic trajectories.

[31] One explanation for the limitation of trajectories between June and September could be that we limit the trajectories to 10 days back in time, because of excessive errors that can arise when trajectories are calculated for longer periods. Since winds are generally lighter over the Pacific in the summer and fall compared to the winter and spring, [*Liang et al.*, 2004], transport from the Asian continent can take longer than 10 days, thus preventing trajectories from classifying an air mass as "Asian." HYSPLIT kinematic back trajectories from three events in the summer and early fall (12 July 2001, 16 July 2001, and 28 September 2001) were inspected for this phenomenon. Trajectories from 12 July 2001 (LRT > 75% = 48 hours) showed that air masses originated over the North Pole and Alaska, suggesting that the 10-day trajectory limit was not an issue for this event. Likewise, trajectories from 28 September 2001 (LRT > 75%, 78 hours) did not cross east of 160°W after 10 days and originated mainly from Alaska. Trajectories from the 16 July 2001 event (LRT > 75% = 54 hours), however, terminated in the North Pacific around 170°E, suggesting that had we been able to follow the air mass back more than 10 days, it may have originated over Asia. Thus, while it seems that slower transport may put 10-day trajectories at a disadvantage compared with GEOS-CHEM, this effect does not explain all of events that were missed by trajectories.

[32] In addition to the lack of "Asian" trajectories between June and September, there appear to be several misclassified "Asian" isentropic trajectories throughout the year. This leads to the result shown in Figure 5a, where Asian CO is actually smaller than ST CO in November and December. To verify that this is caused by misclassified "Asian" trajectories and not misclassified "ST" trajectories, we compared the "Asian" time periods to the GEOS-CHEM results and CO measurements for each month. This is shown in Table 6, where "Asian" isentropic trajectories are grouped into "agreement" and "disagreement" categories, on the basis of whether they corresponded to LRT > 75% or LRT < 25% classifications, respectively. The most disagreement occurred in November, with one-half (48 out of 96) the total "Asian" hours corresponding to LRT < 25%. The average measured CO concentration during these times was 11 ppbv less than the marine mean, suggesting that Asian pollution events were not occurring when "Asian" isentropic trajectories were being classified, in agreement

Table 6. A Comparison of Two Types of Disagreements in Classifications Using Isentropic Trajectories and GEOS-CHEM[a]

Month	"Asian" Isentropic Trajectories by Month, hours	"Agreements" ("Asian" Isentropic and "LRT > 75%")		"Disagreements" ("Asian" Isentropic and "LRT < 25%")	
		Hours	ΔCO_{meas}, ppb	Hours	ΔCO_{meas}, ppb
Jan.	48	12	13		
Feb.	156	36	5	12	−7
March	102	60	12	9	−9
April	60	36	15	6	−13
May	42	42	10	–	–
June	0	–	–	–	–
July	12	12	0	–	–
Aug.	0	–	–	–	–
Sept.	0	–	–	–	–
Oct.	96	36	ND	–	–
Nov.	96	24	−5	48	−11
Dec.	156	48	5	36	−6

[a] ΔCO_{meas} represents the average change from the monthly marine mean during the number of hours of each case. Dashes correspond to no occurrences of a disagreement, and ND refers to no CO measurements.

with GEOS-CHEM. Only 24 out of 96 hours were classified as "Asian" and "LRT > 75%" in November, thus explaining why Asian CO was about 10 ppbv lower than ST CO, shown in the inset of Figure 5a. December, February, March, and April also had some occurrences of "Asian" and "LRT < 25%," although less than November. In each case, the measured CO value is much less than the monthly mean, suggesting a misclassification. In contrast, during times of agreement between isentropic trajectories and GEOS-CHEM ("Asian" and "LRT > 75%"), measured CO is nearly always above the means. Some of the disagreement periods gave trajectories that originated at altitudes higher than 2 km over Asia, raising the possibility that the air masses were effectively isolated from the surface emissions. It would seem that this type of trajectory, a so-called "clean Asian," is more likely to occur in the fall and winter.

[33] In addition to seasonal/monthly differences between GEOS-CHEM and trajectories, a series of events from April–May 2001 shows important short-term inconsistencies as well. Figure 6 shows the time series measurements of CO and O_3, model-calculated LRT, oxidation-CO, and NA from GEOS-CHEM, and isentropic and HYSPLIT

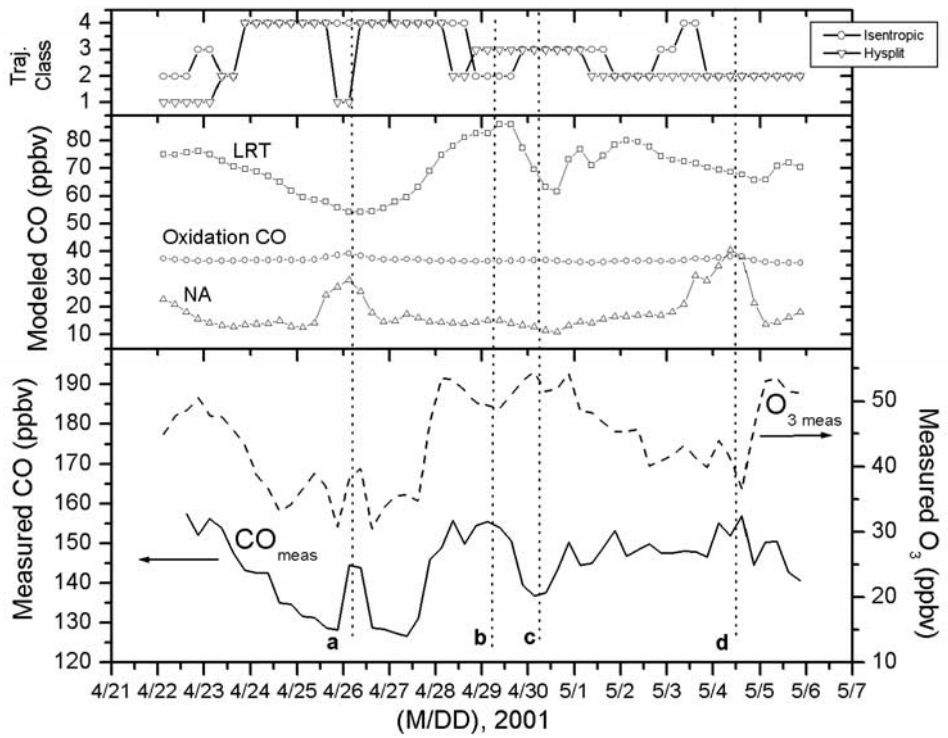

Figure 6. CO and O_3 measurements from a two-week period in April/May 2001, compared with GEOS-CHEM model results and isentropic and HYSPLIT trajectory classifications. No "marine-only" screening was done to these data. Trajectory classifications were given numbers: 1, local; 2, North Pacific (NP); 3, Asian (As); 4, subtropical (ST). See Figure 1 for region definitions. Events a, b, c, and d are specific comparison periods discussed in the text.

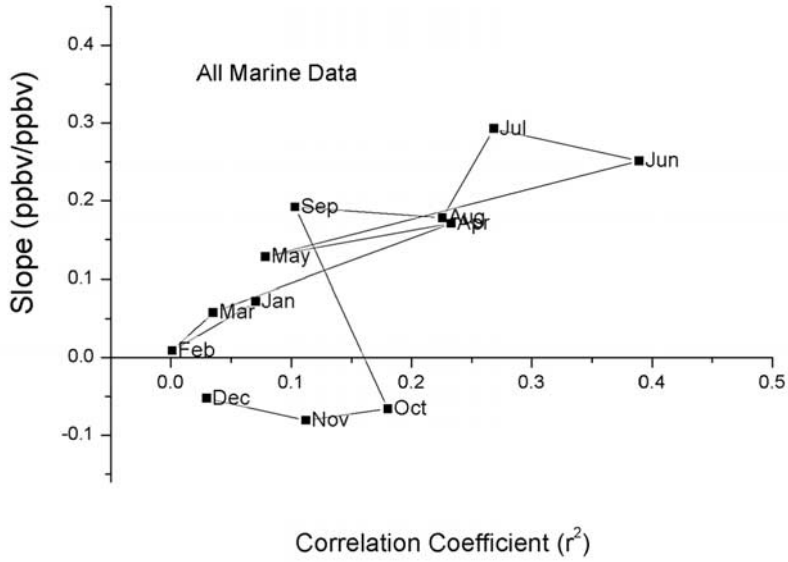

Figure 7. Slope ($\Delta O_3/\Delta CO$ in ppbv/ppbv) versus correlation coefficient r^2 from "marine-only" measured O_3 and CO 6-hour averages by month.

trajectory classifications. These data have not been segregated by the "marine-only" criteria. One difference shown is in the classification of locally influenced air. GEOS-CHEM predicts two small, but significant peaks in NA (events a and d in Figure 6), which are reflected in the measurements (both CO and O_3 show increases). Isentropic trajectories classified these periods as "subtropical" and "North Pacific," and HYSPLIT classified them as "local" and "North Pacific." For both these events, HYSPLIT and isentropic trajectories showed that the backward path of the air masses stayed close to 124°W (the "local" boundary), came up from the south and probably picked up pollutants from Portland, Oregon and other smaller coastal cities.

[34] Events b and c compare the abilities of GEOS-CHEM and trajectories to classify periods of long-range transport. During event b the measured CO rise corresponds to a peak in LRT. HYSPLIT classifies this time as "Asian," whereas isentropic trajectories do not. In event c both trajectory models predict an Asian influence, while LRT and the CO measurements show significant decreases here. GEOS-CHEM more accurately (though not perfectly) captures this event.

3.6. Correlations Between O_3 and CO

[35] The degree of correlation between O_3 and CO can give information on the extent to which O_3 is being photochemically produced from primary pollutants that are coemitted with CO [*Chin et al.*, 1994; *Atherton et al.*, 1996; *Parrish et al.*, 1998; *Mauzerall et al.*, 2000]. The slope obtained from an O_3-CO plot is related to the photochemical production efficiency of O_3 in the pollution plume, and the length of time since pollution emissions. Values of 0.3–0.4 O_3 ppbv/CO ppbv are typical for air masses recently influenced by industrial emissions [*Chin et al.*, 1994; *Parrish et al.*, 1998]. *Price et al.* [2004] observed lower values during the spring at CPO, where dilution and other processes affecting O_3 have more time to occur. In Figure 7 we show the O_3-CO slopes ("marine-only" data) as a function of the square of the correlation coefficient (r^2) at CPO for the entire year. The general pattern of this plot is roughly in the shape of the letter "C," where April–September produce the largest positive correlations, January–March are only slightly positive, and October–December show slight negative correlations. This is consistent with the results shown in Figure 4, where O_3 and CO are both enhanced during periods of LRT > 75% in the spring and summer, whereas CO is enhanced and O_3 is lowered during November and December. This seasonal correlation pattern is analogous to that of *Parrish et al.* [1998], although their data from Sable Island, Canada, produced much greater correlations, both positive and negative, because of closer proximity to pollution sources.

3.7. Diurnal Cycles of O_3

[36] O_3 concentrations from "marine-only" data averaged by local time of day for each two-month period during the year are shown in Figure 8. May–June and September–October are shown as individual months since seasonal changes in O_3 during these times of the year can overwhelm any diurnal variability. Diurnal cycles of CO are not discernible above background variations in any season and are not shown. Notice the consistent O_3 diurnal patterns in the plots covering March through August, which show a rise of ~2–4 ppbv during the sunlit hours (0800–2000 local time (LT)). Diurnal land-sea breezes are not a factor since all data have been segregated by wind direction. These diurnal patterns are consistent with net photochemical production, which would require a local source of NO_x. The amount of NO_x needed to generate our observed O_3 production rate of 2–4 ppbv/d is on the order of 100–250 pptv [*Liu et al.*, 1987; *Herring et al.*, 1997]. Measurements of NO_x at CPO by *Jaffe et al.* [2001] show a March–April average of 189 pptv of NO_x, but with high variability, consistent with the range required to produce our observed daily production of O_3. *Jaffe et al.* [2001] highlight the importance of oceangoing ships in controlling

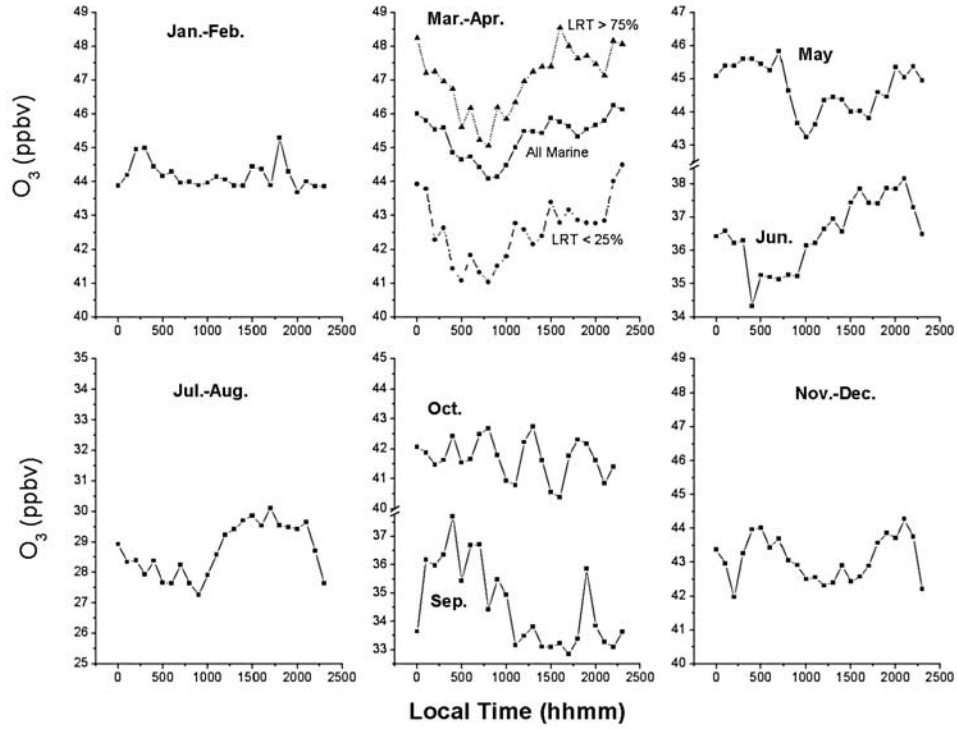

Figure 8. Diurnal cycles of "marine-only" measured O_3. LRT-segregated data are shown for March and April only.

NO_x levels at CPO (due to the close proximity of the Straits of Juan de Fuca). Ships may also be an important influence on the NO_x budget of the remote MBL [*Lawrence and Crutzen*, 1999], which should be largely independent of season since shipping occurs throughout the year. Thus O_3 production at CPO would mainly depend on available sunlight, being highest in the summer, lowest in the winter. Our results in Figure 8 are fairly consistent with this hypothesis; O_3 daily production is limited to the months with the greatest amount of sunlight, highest temperatures, and the least amount of cloud cover. The only exception is September and October, which show no apparent pattern. Thus, in these months, there are evidently other processes interfering with daily production of O_3, even though climatologically, September and October provide as much sunlight as during the spring. One explanation is that peroxyacetyl nitrate (PAN) from long-range transport is a significant source of NO_x in the spring but not in the fall [*Kotchenruther et al.*, 2001b].

[37] However, an LRT segregation of the data does not appear to influence the diurnal variability of O_3 at CPO. This can be seen in the March–April panel of Figure 8, which compares the diurnal cycles from all marine, LRT > 75% and LRT < 25% segregated data. For simplicity, only the results from March–April are shown, although the data from other months is similar. Since the magnitude and phase of the diurnal cycles from both LRT categories is comparable, this again points to a local source of NO_x (i.e., ships) as the dominant factor for the net O_3 production that we observe. Although there is much debate currently over the degree to which ship emissions influence the relatively pristine MBL [*Song et al.*, 2003, and references therein], our previous data [*Jaffe et al.*, 2001] suggest that CPO is under that influence. Thus future O_3 measurements at CPO during the spring and summer should be viewed with this influence in mind.

4. Conclusions

[38] In this work, CO and O_3 concentrations were analyzed, along with results from the GEOS-CHEM global chemical transport model and two types of back trajectories. The data from a full annual cycle allow us to determine the influence of long-range-transported pollution on the seasonality of CO and O_3. Using GEOS-CHEM, a quantity called "LRT" is obtained, which represents the amount of CO produced from Asian biomass burning, and Asian + European fossil fuel and biofuel sources. LRT correlates well with measured CO and thus allows for segregation of the CO and O_3 data into "more polluted" and "less polluted" categories (>75th percentile and <25th percentile, respectively, of each month's worth of LRT data). The difference in measured CO and O3 between these two categories gives a measure of the net Asian enhancement above the background, which shows a maximum for CO (23 ppbv) during January–June and a maximum for O_3 (4.4 ppbv) during April–October. This shift in the timing of the O_3 maximum suggests that while long-range transport of pollutants is strongest early in the year, maximum O_3 enhancement comes later, which may reflect changing O_3 production rates at the source regions.

[39] The LRT parameter from GEOS-CHEM was used to identify specific long-range transport events at CPO.

Criteria consisted of at least 24 hours of LRT >75th percentile during the event, a positive model-measurement CO correlation and a statistically significant increase ($P > 0.95$) in measured and total modeled CO. Events occurred throughout the year, with the strongest ones in winter and spring (measured CO enhanced >20 ppbv above the mean). The time-weighted average enhancement for all 16 events is 16 ppbv for CO and 0.4 ppbv for O_3. The predicted enhancement of total modeled CO is 17 ppbv, indicating that on average, the model does an excellent job of quantifying these events. O_3 behavior appeared complicated, with no apparent pattern of enhancement in any season. Some events with enhanced CO also had large O_3 enhancements, and were associated with dry air intrusions, suggesting a stratospheric influence on O_3 levels. Another six events were predicted by GEOS-CHEM, but did not show good agreement with the observations. In most of these cases, GEOS-CHEM accurately predicted the magnitude of the CO enhancements, but missed the timing of the CO maximum, thus leading to a poor measurement-model correlation.

[40] The ability of LRT to classify CO/O_3 measurements is compared with both isentropic and HYSPLIT modeled vertical velocity back trajectories. The methods generally agree during the spring, in terms of the magnitude of enhancement from the ''more polluted'' versus the ''less polluted'' categories (20–30 ppbv for CO and 0–6 ppbv for O_3). However, important differences in all seasons were also highlighted. In particular, summer trajectories provided little information because only one ''Asian'' isentropic trajectory was classified between June and September. Both HYSPLIT kinematic and isentropic trajectories completely missed an ''Asian'' pollution event, which occurred around 12 July 2001. GEOS-CHEM was able to segregate the summertime measurements with some accuracy, showing a significant distant pollution influence on O_3. During the fall, there were several ''Asian'' trajectories with levels of CO below the background, which were accurately predicted by GEOS-CHEM. Furthermore, during a particular spring period, GEOS-CHEM displayed better spatial and temporal resolution than trajectories by identifying periods of local and Asian influence when trajectories classified the air masses as the marine background.

[41] Correlations between measured O_3 and CO, which are used as a measure of the relative quantity of O_3 produced from anthropogenic emissions, are generally weak throughout the year reflecting the mixing with cleaner source regions and the complex chemistry of O_3. However, April–August show the strongest correlations, $r^2 = 0.2–0.4$, $\Delta O_3/\Delta CO = 0.2–0.3$, which is consistent with the GEOS-CHEM results.

[42] Finally, diurnal cycles of O_3 during the spring and summer show a consistent concentration increase during the daytime, suggesting photochemical production. NO_x values measured in the spring are high enough to produce O_3 at the observed rates (2–4 ppbv/d). This NO_x presumably comes from ships that enter and exit the Straits of Juan de Fuca. Diurnal patterns from LRT > 75% and LRT > 25% segregated data have the same phase and magnitude, which is consistent with this hypothesis.

[43] **Acknowledgments.** This work was supported by the National Science Foundation. We thank the Makah Nation for allowing us to sample the atmosphere on their lands. James Dennison constructed the map used in this paper. The GEOS-CHEM model is managed by the Atmospheric Chemistry Modeling Group at Harvard University with support from the NASA Atmospheric Chemistry Modeling and Analysis Program.

References

Abbot, D. S., P. I. Palmer, R. V. Martin, K. V. Chance, D. J. Jacob, and A. Guenther (2003), Seasonal and interannual variability of North American isoprene emissions as determined by formaldehyde column measurements from space, *Geophys. Res. Lett.*, *30*(17), 1886, doi:10.1029/2003GL017336.

Anderson, T. L., D. S. Covert, J. D. Wheeler, J. M. Harris, K. D. Perry, B. E. Trost, and D. A. Jaffe (1999), Aerosol backscatter fraction and single scattering albedo: Measured values and uncertainties at a coastal station in the Pacific Northwest, *J. Geophys. Res.*, *104*, 26,793–26,807.

Atherton, C. S., S. Sillman, and J. Walton (1996), Three-dimensional global modeling studies of the transport and photochemistry over the North Atlantic Ocean, *J. Geophys. Res.*, *101*, 29,289–29,304.

Barth, M. C., P. G. Hess, and S. Madronich (2002), Effect of marine boundary layer clouds on tropospheric chemistry as analyzed in a regional chemistry transport model, *J. Geophys. Res.*, *107*(D11), 4126, doi:10.1029/2001JD000468.

Bertschi, I. T., D. A. Jaffe, L. Jaeglé, H. U. Price, and J. B. Dennison (2004), PHOBEA/ITCT 2002 airborne observations of transpacific transport of ozone, CO, volatile organic compounds, and aerosols to the northeast Pacific: Impacts of Asian anthropogenic and Siberian boreal fire emissions, *J. Geophys. Res.*, *109*, D23S12, doi:10.1029/2003JD004328, in press.

Bey, I., D. J. Jacob, J. A. Logan, and R. M. Yantosca (2001a), Asian chemical outflow to the Pacific in spring: Origins, pathways, and budgets, *J. Geophys. Res.*, *106*, 23,097–23,113.

Bey, I., D. J. Jacob, R. M. Yantosca, J. A. Logan, B. D. Field, A. M. Fiore, Q. Li, H. Y. Liu, L. J. Mickley, and M. G. Schultz (2001b), Global modeling of tropospheric chemistry with assimilated meteorology: Model description and evaluation, *J. Geophys. Res.*, *106*, 23,073–23,096.

Carmichael, G. R., I. Uno, M. J. Phadnis, Y. Zhang, and Y. Sunwoo (1998), Tropospheric ozone production and transport in the springtime in east Asia, *J. Geophys. Res.*, *103*, 10,649–10,671.

Chin, M., D. J. Jacob, J. W. Munger, D. D. Parrish, and B. G. Doddridge (1994), Relationship of ozone and carbon monoxide over North America, *J. Geophys. Res.*, *99*, 14,565–14,573.

Derwent, R. G., P. G. Simmonds, S. Seuring, and C. Dimmer (1998), Observation and interpretation of the seasonal cycles in the surface concentrations of ozone and carbon monoxide at Mace Head, Ireland from 1990 to 1994, *Atmos. Environ.*, *32*, 145–157.

Dickerson, R. R., K. P. Rhoads, T. P. Carsey, S. J. Oltmans, J. P. Burrows, and P. J. Crutzen (1999), Ozone in the remote marine boundary layer: A possible role for halogens, *J. Geophys. Res.*, *104*, 21,385–21,395.

Duncan, B. N., R. V. Martin, A. C. Staudt, R. Yevich, and J. A. Logan (2003), Interannual and seasonal variability of biomass burning emissions constrained by satellite observations, *J. Geophys. Res.*, *108*(D2), 4100, doi:10.1029/2002JD002378.

Elliott, S., D. R. Blake, R. A. Duce, C. A. Lai, I. McCreary, L. A. McNair, F. S. Rowland, A. G. Russell, G. E. Streit, and R. P. Turco (1997), Motorization of China implies changes in Pacific air chemistry and primary production, *Geophys. Res. Lett.*, *24*, 2671–2674.

Fiore, A. M., D. J. Jacob, I. Bey, R. M. Yantosca, B. D. Field, A. C. Fusco, and J. G. Wilkinson (2002), Background ozone over the United States in summer: Origin, trend, and contribution to pollution episodes, *J. Geophys. Res.*, *107*(D15), 4275, doi:10.1029/2001JD000982.

Fuelberg, H. E., R. O. Loring Jr., M. V. Watson, M. C. Sinha, K. E. Pickering, A. M. Thompson, G. W. Sachse, D. R. Blake, and M. R. Schoeberl (1996), TRACE A trajectory intercomparison: 2. Isentropic and kinematic methods, *J. Geophys. Res.*, *101*, 23,927–23,939.

Fuelberg, H. E., C. M. Kiley, J. R. Hannan, D. J. Westberg, M. A. Avery, and R. E. Newell (2003), Meteorological conditions and transport pathways during the Transport and Chemical Evolution Over the Pacific (TRACE-P) experiment, *J. Geophys. Res.*, *108*(D20), 8782, doi:10.1029/2002JD003092.

Harris, J. M., and J. D. W. Kahl (1994), An analysis of 10-day isentropic flow patterns for Barrow, Alaska: 1985–1992, *J. Geophys. Res.*, *99*, 25,845–25,855.

Harris, J. M., E. J. Dlugokencky, S. J. Oltmans, P. P. Tans, T. J. Conway, P. C. Novelli, and K. W. Thoning (2000), An interpretation of trace gas correlations during Barrow, Alaska, winter dark periods, 1986–1997, *J. Geophys. Res.*, *105*, 17,267–17,278.

He, S., and G. R. Carmichael (1999), Sensitivity of photolysis rates and ozone production in the troposphere to aerosol properties, *J. Geophys. Res.*, *104*, 26,307–26,324.

Herring, J. A., D. A. Jaffe, H. J. Beine, S. Madronich, and D. R. Blake (1997), High-latitude springtime photochemistry. Part II: Sensitivity studies of ozone production, *J. Atmos. Chem.*, *27*, 155–178.

Holloway, T., H. Levy II, and P. Kasibhatla (2000), Global distribution of carbon monoxide, *J. Geophys. Res.*, *105*, 12,123–12,147.

Huebert, B. J., T. Bates, P. B. Russell, G. Shi, Y. J. Kim, K. Kawamura, G. Carmichael, and T. Nakajima (2003), An overview of ACE-Asia: Strategies for quantifying the relationships between Asian aerosols and their climatic impacts, *J. Geophys. Res.*, *108*(D23), 8633, doi:10.1029/2003JD003550.

Jacob, D. J., J. A. Logan, and P. P. Murti (1999), Effect of rising Asian emission on surface ozone in the United States, *Geophys. Res. Lett.*, *26*, 2175–2178.

Jacob, D. J., J. H. Crawford, M. M. Kleb, V. E. Connors, R. J. Bendura, J. L. Raper, G. W. Sachse, J. C. Gille, L. Emmons, and C. L. Heald (2003), The Transport and Chemical Evolution Over the Pacific (TRACE-P) mission: Design, execution, and overview of results, *J. Geophys. Res.*, *108*(D20), 9000, doi:10.1029/2002JD003276.

Jaeglé, L., D. A. Jaffe, H. U. Price, P. Weiss-Penzias, P. I. Palmer, M. J. Evans, D. J. Jacob, and I. Bey (2003), Sources and budgets for CO and O_3 in the northeastern Pacific during the spring of 2001: Results from the PHOBEA-II experiment, *J. Geophys. Res.*, *108*(D20), 8802, doi:10.1029/2002JD003121.

Jaffe, D. A., L. N. Yurganov, E. Pullman, J. Reuter, A. Mahura, and P. C. Novelli (1998), Measurements of CO and O_3 at Shemya, Alaska, *J. Geophys. Res.*, *103*, 1493–1502.

Jaffe, D. A., et al. (1999), Transport of Asian air pollution to North America, *Geophys. Res. Lett.*, *26*, 711–714.

Jaffe, D. A., T. Anderson, D. Covert, B. Trost, J. Danielson, W. Simpson, D. Blake, J. Harris, and D. Streets (2001), Observations of ozone and related species in the northeast Pacific during the PHOBEA campaigns: 1. Ground-based observations at Cheeka Peak, *J. Geophys. Res.*, *106*, 7449–7461.

Jaffe, D. A., I. McKendry, T. Anderson, and H. Price (2003a), Six 'new' episodes of trans-Pacific transport of air pollutants, *Atmos. Environ.*, *37*, 391–404.

Jaffe, D., H. Price, D. Parrish, A. Goldstein, and J. Harris (2003b), Increasing background ozone during spring on the west coast of North America, *Geophys. Res. Lett.*, *30*(12), 1613, doi:10.1029/2003GL017024.

Kotchenruther, R. A., D. A. Jaffe, H. J. Beine, T. L. Anderson, J. W. Bottenheim, J. M. Harris, D. R. Blake, and R. Schmitt (2001a), Observations of ozone and related species in the northeast Pacific during the PHOBEA campaigns: 2. Airborne observations, *J. Geophys. Res.*, *106*, 7463–7483.

Kotchenruther, R., D. Jaffe, and L. Jaeglé (2001b), Ozone photochemistry and the role of peroxyacetyl nitrate in the springtime northeastern Pacific troposphere: Results from the Photochemical Ozone Budget of the Eastern North Pacific Atmosphere (PHOBEA) campaign, *J. Geophys. Res.*, *106*, 28,731–28,742.

Kunz, H., and P. Speth (1997), Variability of near-ground ozone concentrations during cold front passages: A possible effect of tropopause folding events, *J. Atmos. Chem.*, *28*, 77–95.

Langmann, B., S. E. Bauer, and I. Bey (2003), The influence of the global photochemical composition of the troposphere on European summer smog, Part I, Application of a global to mesoscale model chain, *J. Geophys. Res.*, *108*(D4), 4146, doi:10.1029/2002JD002072.

Lawrence, M. G., and P. J. Crutzen (1999), Influence of NO_x emissions from ships on tropospheric photochemistry and climate, *Nature*, *402*, 167–170.

Lelieveld, J., and F. J. Dentener (2000), What controls tropospheric ozone?, *J. Geophys. Res.*, *105*, 3531–3551.

Li, Q., et al. (2002), Transatlantic transport of pollution and its effects on surface ozone in Europe and North America, *J. Geophys. Res.*, *107*(D13), 4166, doi:10.1029/2001JD001422.

Liang, Q., L. Jaeglé, D. A. Jaffe, P. Weiss-Penzias, A. Heckman, and J. A. Snow (2004), Long-range transport of Asian pollution to the northeast Pacific: Seasonal variations and transport pathways of carbon monoxide, *J. Geophys. Res.*, *109*, D23S07, doi:10.1029/2003JD004402, in press.

Liu, H., D. J. Jacob, I. Bey, R. M. Yantosca, B. N. Duncan, and G. W. Sachse (2003), Transport pathways for Asian pollution outflow over the Pacific: Interannual and seasonal variations, *J. Geophys. Res.*, *108*(D20), 8786, doi:10.1029/2002JD003102.

Liu, S. C., M. Trainer, F. C. Fehsenfeld, D. D. Parrish, E. J. Williams, D. W. Fahey, G. Hubler, and P. C. Murphy (1987), Ozone production in the rural troposphere and the implications for regional and global ozone distributions, *J. Geophys. Res.*, *92*, 4191–4207.

Mauzerall, D. L., D. Narita, H. Akimoto, L. Horowitz, S. Walters, D. Hauglustaine, and G. Brasseur (2000), Seasonal characteristics of tropospheric ozone production and mixing ratios over east Asia: A global three-dimensional chemical transport model analysis, *J. Geophys. Res.*, *105*, 17,895–17,910.

Merrill, J. T. (1994), Isentropic airflow probability analysis, *J. Geophys. Res.*, *99*, 25,881–25,889.

Moody, J. L., S. J. Oltmans, H. Levy II, and J. T. Merrill (1995), Transport climatology of tropospheric ozone: Bermuda, 1988–1991, *J. Geophys. Res.*, *100*, 7179–7194.

Newell, R. E., and M. J. Evans (2000), Seasonal changes in pollutant transport to the North Pacific: The relative importance of Asian and European sources, *Geophys. Res. Lett.*, *27*, 2509–2512.

Novelli, P. C., L. P. Steele, and P. P. Tans (1992), Mixing ratios of carbon monoxide in the troposphere, *J. Geophys. Res.*, *97*, 20,731–20,750.

Novelli, P. C., K. A. Masarie, and P. M. Lang (1998), Distributions and recent changes of carbon monoxide in the lower troposphere, *J. Geophys. Res.*, *103*, 19,015–19,033.

Oltmans, S. J., and H. Levy II (1994), Surface ozone measurements from a global network, *Atmos. Environ.*, *28*, 9–24.

Parrish, D. D., M. Trainer, J. S. Holloway, J. E. Yee, M. S. Warshawsky, F. C. Fehsenfeld, G. L. Forbes, and J. L. Moody (1998), Relationships between ozone and carbon monoxide at surface sites in the North Atlantic region, *J. Geophys. Res.*, *103*, 13,357–13,376.

Pickering, K. E., A. M. Thompson, D. P. McNamara, M. R. Schoeberl, H. E. Fuelberg, R. O. Loring Jr., M. V. Watson, K. Fakhruzzaman, and A. S. Bachmeier (1996), TRACE A trajectory intercomparison: 1. Effects of different input analyses, *J. Geophys. Res.*, *101*, 23,909–23,925.

Pochanart, P., H. Akimoto, Y. Kajii, V. M. Potemkin, and T. V. Khodzher (2003), Regional background ozone and carbon monoxide variations in remote Siberia/east Asia, *J. Geophys. Res.*, *108*(D1), 4028, doi:10.1029/2001JD001412.

Price, H. U., D. A. Jaffe, P. V. Doskey, I. McKendry, and T. Anderson (2003), Vertical profiles of O_3, aerosols, CO and NMHCs in the northeast Pacific during the TRACE-P and ACE-Asia experiments, *J. Geophys. Res.*, *108*(D20), 8799, doi:10.1029/2002JD002930.

Price, H. U., D. A. Jaffe, O. R. Cooper, and P. V. Doskey (2004), Photochemistry, ozone production, and dilution during long-range transport episodes from Eurasia to the northwest United States, *J. Geophys. Res.*, *109*, D23S13, doi:10.1029/2003JD004400, in press.

Simmonds, P. G., S. Seuring, G. Nickless, and R. G. Derwent (1997), Segregation and interpretation of ozone and carbon monoxide measurements by air mass origin at the TOR station Mace Head, Ireland from 1987 to 1995, *J. Atmos. Chem.*, *28*, 45–59.

Song, C. H., G. Chen, S. R. Hanna, J. Crawford, and D. D. Davis (2003), Dispersion and chemical evolution of ship plumes in the marine boundary layer: Investigation of $O_3/NO_y/HO_x$ chemistry, *J. Geophys. Res.*, *108*(D4), 4143, doi:10.1029/2002JD002216.

Staudt, A. C., D. J. Jacob, J. A. Logan, D. Bachiochi, T. N. Krishnamurti, and G. W. Sachse (2001), Continental sources, transoceanic transport, and interhemispheric exchange of carbon monoxide over the Pacific, *J. Geophys. Res.*, *106*, 32,571–32,590.

Stohl, A. (1998), Computation, accuracy and applications of trajectories: A review and bibliography, *Atmos. Environ.*, *32*, 947–966.

Streets, D. G., and S. T. Waldhoff (2000), Present and future emissions of air pollutants in China: SO_2, NO_x, and CO, *Atmos. Environ.*, *34*, 363–374.

Weiss-Penzias, P., D. A. Jaffe, A. McClintick, E. M. Prestbo, and M. S. Landis (2003), Gaseous elemental mercury in the marine boundary layer: Evidence for rapid removal in anthropogenic pollution, *Environ. Sci. Technol.*, *37*, 3755–3763.

Yienger, J. J., M. Galanter, T. A. Holloway, M. J. Phandis, S. K. Guttikinda, G. R. Carmichael, W. J. Moxim, and H. Levy II (2000), The episodic nature of air pollution transport from Asia to North America, *J. Geophys. Res.*, *105*, 26,931–26,945.

L. Jaeglé and Q. Liang, Department of Atmospheric Sciences, University of Washington, Seattle, Box 351640, Seattle, WA 98195-1640, USA. (jaegle@atmos.washington.edu; qing@atmos.washington.edu)

D. A. Jaffe and P. Weiss-Penzias, Interdisciplinary Arts and Sciences, University of Washington, Bothell, 18115 Campus Way NE, Box 358530, Bothell, WA 98011, USA. (djaffe@u.washington.edu; pweiss@bothell.washington.edu)